ACS OMEGA

Open Access

http://pubs.acs.org/journal/acsodf

Article

Synthesis and Mechanical Performances of Polyurethane Bio-Based Adhesives Resulted from the Depolymerization of Lignocellulose Biomass

Edina Rusen, Gabriela Toader, Aurel Diacon, Florin Marian Dîrloman, Liviu Cristian Matache, Florentina Alexe, Adrian Dinescu, and Alexandra Mocanu*

Cite This: *ACS Omega* 2023, 8, 38178−38190

Read Online

ACCESS | Metrics & More | Article Recommendations | Supporting Information

ABSTRACT: The purpose of this study is to valorize biomass waste into products with added value for indoor applications. Thus, broadleaf sawdust was chemically processed by the solvolysis reaction in acid catalysis in the presence of diethylene glycol at 160 °C for 4 h. After filtration and removal of the unreacted biomass, the glycolysis product was used in 6 different polyurethane adhesive formulations for wood bonding. The adhesive films were characterized by FT-IR, TGA, and DMA, while the mechanical performances were investigated by tensile and three-point bending tests. An innovative method for the determination of the working time was proposed. After the displacement of the wood substrates by the tensile test, the bonded area was investigated by SEM analysis. To confirm a correlation between the mechanical performances of the adhesives and their structure/formulation, two-dimensional (2D) simulations were performed based on the tensile tests.

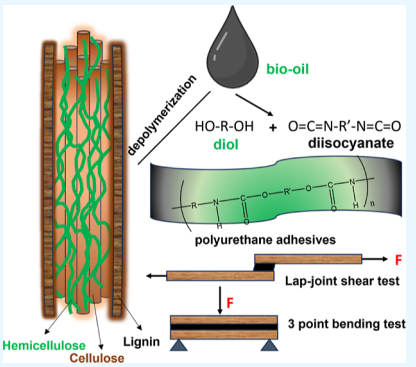

1. INTRODUCTION

Nowadays, there are several definitions for the "biomass" term that have different meanings depending on the circumstances. For instance, in ecology, biomass is defined as the weight or total quantity of living organisms of one animal or plant species (biomass species) or of all the species in a community/habitat, while in the bioenergy field, biomass is related to the matter from recently living but not dead organisms.[1]

According to Directive 2009/28/EC defined by the European Parliament and Council, the term biomass has a larger meaning describing the biodegradable fraction of products, including wastes and residues from different industries such as agriculture, forestry, fisheries, and aquaculture, industrial and municipal1 waste of biological origin associated to energy/fuel production.[2−5]

Biomass is the main renewable energy source in the European Union (EU) for cleaner and more effective energy plans in the short and long terms (2030 and 2050).[6−8] Therefore, the necessity for new biomass processing strategies and EU REACH compliant policies prompted researchers to develop more innovative bio-based products.[9,10]

The need to get independent from the fossil resources led to the development of different strategies for lignocellulose biomass processing, such as extrusion, sonication, milling, steam explosion, ammonia explosion, supercritical CO_2 explosion, organosolv, ozonolysis, hydrolysis, enzymatic hydrolysis, alkali or acid pretreatment, oxidation, ionic liquid, and microwave-assisted methods.[11−13]

The abundance of lignin in nature and its distinctive structure, which is based on electron-rich aromatic rings, have drawn interest in a range of chemical techniques for its decomposition into smaller compounds.[14] Thus, in terms of manufacturing new innovative products, the aromatic structure of lignin was treated by oxidation, demethylation, hydroxymethylation, phenolysis, liquefaction, etc. due to its relatively low reactivity and its non-uniform structure attributed to the origin of lignin (i.e., softwood, hardwood, or graminaceous plants).[15−18] Therefore, the main purpose is to create more reactive hydroxyl groups susceptible to react with other compounds like tannin, aldehyde, or isocyanates[15] to develop "greener" products like foams, resins, or adhesives.[15,17]

Regardless of their chemical structure, the global market for adhesives is predicted to approach 21 billion USD by 2024.[19] The main issue concerning these products is related with the formaldehyde-based formulations that are proven to affect the environment and human health due to the formaldehyde emissions.[19]

Thus, bicomponent PUR adhesive chemistry is nowadays in a transition to formaldehyde-free adhesives in which polyols

Received: June 20, 2023
Accepted: August 30, 2023
Published: October 5, 2023

Scheme 1. Flow Scheme for Adhesives Formulation, Mechanical, and Process Simulation Testing

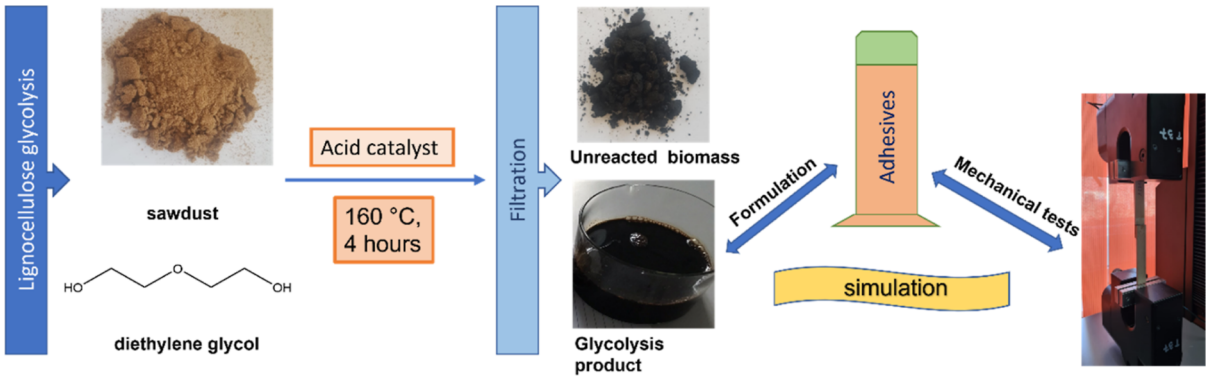

(component A) can be manufactured from renewable resources.[20]

In terms of PUR wood adhesives, the mechanical performances are strongly related to the conditions necessary to obtain bio-polyols with suitable properties such as hydroxyl number or viscosity.[15,21] Thus, the reaction conditions involve a rigorous control of some parameters such as: (i) the moisture content of the raw lignocellulose material (i.e., a drying process must be applied), (ii) solvent type, (iii) the catalyst and catalyst concentration, (iv) process temperature, and (v) reaction time.[20,21]

For instance, Gosz et al.[22] obtained bio-polyols with varying hydroxyl number in the range of 214−687 mg KOH/g at 120, 150, and 170 °C in the presence of glycerol and poly(ethylene glycol) derivatives as solvents after 6 h, proving higher conversion of lignocellulose biomass with higher temperatures. Similar results were obtained by Lee et al.[23] that depolymerized the lignocellulose biomass *Taiwan acacia* and *China fir* in acid catalysis in a mixture of glycerol and poly(ethylene glycol). The final products were reacted with three different diisocyanates to develop PUR adhesives with different properties in terms of gel time and bonding strength.

Previous studies demonstrated that the main advantage of PUR adhesives based on bio-polyols from the liquefaction of lignocellulosic biomass is related with the abundant availability of the raw materials (mostly forestry or agricultural wastes), the richness of hydroxyl groups of the bio-oil, and the (thermal and mechanical) stability of the aromatic PUR structure of the final product.[18,22,24]

Considering the abovementioned advantages, our study was focused on two directions: (a) the development of bio-polyols obtained by glycolysis of broadleaf saw dust and (b) the manufacturing process of PUR adhesives for wood bonding. In this study, the broad leaf biomass was subjected to drying to ensure that the moisture content was below 5% before the liquefaction process. Scheme 1 describes in detail the most important steps of our study.

One of the main goals of this study is to develop a higher value-added alternative for forestry waste processing, considering that sawdust is mostly used in our country as a filling agent in wood-based composite products for the civil engineering industry or as briquettes for igniting fire.

The novelty of this study resides in the valorization of broadleaf sawdust for the obtaining of bio-polyols by glycolysis using diethylene glycol (DEG). The obtained bio-polyols were employed in 6 bicomponent polyurethane formulations for wood adhesives. Standard three-point bending was carried out in two modes, and tensile testing was used experimentally to determine the mechanical performance of the adhesives.

To characterize the synthesized adhesives, numerical simulation was performed based on the tensile test experiment. The simulation aims to establish a material model and to determine the material's parameters that lead to the best possible approximation of the experimentally obtained results. This approach is iterative and involves incrementing simulation parameters based on a set of data presented in the specialized literature and the comparison between the theoretically obtained results and the experimental ones.

2. MATERIALS AND METHODS

2.1. Materials. Broadleaf sawdust (from forestry processing, RomSilva, Romania) was dried to 5% wt moisture. Diethylene glycol (DEG) (Merck Romania), H_2SO_4 (98% wt) (Redox Romania), and acetone (Merck Romania) were used as such for the synthesis and separation of glycolysis products.

The bicomponent polyurethane adhesive formulations involved the use of triol polyether-polyol PETOL 46-3MB (hydroxyl index, I_{OH} = 43 ÷ 49 mg KOH/g), polyoxypropylene glycol PETOL 250−2 (hydroxyl index, I_{OH} = 240 ÷ 260 mg KOH/g), and 4,4′-methylene diphenyl diisocyanate (MDI) (Covestro DESMODUR 44V20L, Merck Romania) (NCO content = 30.5 ÷ 32.5%) without further purification.

2.2. Methods. *2.2.1. Synthesis of Glycolysis Products from Lignocellulosic Biomass.* In a typical reaction, 15 g of dried broadleaf sawdust (5% wt moisture) were subjected to glycolysis using 145 g of DEG and an acid catalysis (4 mL of H_2SO_4) for 4 h at 160 °C. At the end of the reaction, the black liquid (85% conversion) was separated from the undegraded lignocellulosic biomass by vacuum filtration. The solid fraction was then washed with 200 mL of distilled water and 20 mL of acetone to remove the water and organic soluble compounds from the cake retained by the filter. The glycolysis product, indexed as **Pol-L**, was dried until a constant mass to remove the water and acetone.

2.2.2. Synthesis of Bicomponent Polyurethane Adhesives. In Table 1, 6 formulations of Pol-L-based polyurethane adhesives (A1 ÷ A6) and their blank counterparts (M1 ÷ M6) and are presented.

3. CHARACTERIZATION

3.1. Determination of the Hydroxyl Index of the Pol-L Glycolysis Product. Hydroxyl number was determined based on the ASTM D4274-99 (standard test methods for testing polyurethane raw materials: determination of hydroxyl

https://doi.org/10.1021/acsomega.3c04393
ACS Omega 2023, 8, 38178−38190

Table 1. Bicomponent Formulations of Polyurethane Adhesives

sample	component A		component B	
	Pol-L, g	PETOL 46-3MB, g	PETOL 250−2, g	MDI, g
M1		2.5	1.5	4.25
M2		2.5	1.5	4
M3		2.5	1.5	3.75
M4		1.5	2.5	4.25
M5		1.5	2.5	4
M6		1.5	2.5	3.75
A1	1	2.5	1.5	4.25
A2	1	2.5	1.5	4
A3	1	2.5	1.5	3.75
A4	1	1.5	2.5	4.25
A5	1	1.5	2.5	4
A6	1	1.5	2.5	3.75

numbers of polyols), method A (acetic anhydride pressure bottle) (described in detail in the Supporting Information).

3.2. FT-IR Analysis of the Pol-L Glycolysis Product and Polyurethane Adhesives. FT-IR analysis of the glycolysis product and polyurethane-based adhesive formulations was performed on a Spectrum Two FT-IR Spectrometer (PerkinElmer), equipped with a universal ATR—MIRacle Single Reflection ATR—PIKE Technologies, at 4 cm^{-1} resolution, from 550 to 4000 cm^{-1} and a buildup of 32 scans.

3.3. TGA Analysis of Pol-L Glycolysis Product and PUR Adhesives. The thermogravimetric analyses (TGA) of the bio-polyol and cured adhesive formulations were performed using Netzsch TG 209 F3 Tarsus equipment, considering the next parameters: nitrogen atmosphere flow rate 20 mL min^{-1}; samples mass ∼4 mg; temperature range: room temperature − 900 °C; heating rate: 10 °C min^{-1} in an alumina (Al_2O_3) crucible.

3.4. Determination of Pot-Life/Working Time of the Polyurethane Adhesive Formulations. The pot life/working time for the developed polyurethane adhesive mixtures was determined using a FLIR A6700 MWIR infrared camera under the following parameters: sample amount: ∼15 g; standard temperature range of the device: −20 to 350 °C. A mechanical mixer was used to stir the polyurethane adhesive formulations at a speed of 150 rpm. Tests were performed at ambient temperature.

3.5. DMA Analysis of the Polyurethane Adhesive Formulations. DMA mechanical tests were performed for all samples on Discovery 850 DMA TA Instruments equipment in single cantilever mode on a temperature ramp varying from −30 to +150 °C with a 5 °C/min heating rate. For this test, after complete curing, the samples were cut to approx. 36 mm × 12 mm × 0.3 mm ± 0.02 mm to determine the values of glass transition temperature (T_g).

3.6. Three-Point Bending Test of the Polyurethane Adhesive Formulations. For all mechanical tests, the wood strips (*Fagus sylvatica* L.) were stored at 20 °C/65% relative humidity until a moisture content of approx. 12% was attained.

The three-point bending test (3PBT) was accomplished in two ways: (a) stress ramp and (b) oscillation mode using the same equipment, Discovery 850 DMA TA Instruments, employing 3-point bending clamps considering an adjustment of the ASTM D790-17 standard on the clamping system of the above-mentioned equipment (the samples were 5 mm wide compared to the standard).

A thin layer of PUR adhesives was brushed on the surface of wood specimens, followed by the overlapping of two wood substrates of 5 mm × 42 mm × 1 mm ± 0.02 mm.

For rate control stress ramp (a), the tests were performed at 25 ± 0.1 °C with a preload force of 0.1 N and a ramp rate of 5 N/min up to 17 N maximal force. The results were compared by plotting the medium values of stress versus strain obtained after the analysis of three specimens for each sample.

For oscillation mode (b), the samples were subjected to sweep mode by varying the amplitude from 1 to 50 μm with a frequency of 1 Hz and a preload force of 0.01 N at 25 ± 0.1 °C.

Analyses were performed in triplicate, and the mean values of storage modulus and loss modulus were plotted versus oscillation strain to compare the Pol-L-based PUR adhesive formulations with blank samples.

All the abovementioned tests were also performed on wood substrates without adhesive.

3.7. Tensile Tests of the Polyurethane Adhesive Formulations. To determine the value of the maximal stress at break, the blank and Pol-L-based PUR adhesives were subjected to tensile tests on the Titan 10 Universal Strength-Testing Machine equipped with a 10,000 N force cell. The tensile tests were performed according to Standard EN 205-2016—wood adhesives for non-structural applications—determination of tensile shear strength of lap joints. In this case, the rectangular-shaped wood substrates (*F. sylvatica* L.) of 20 mm × 150 mm were bonded by a 0.5 ± 0.02 mm layer of PUR adhesive, applied on a 20 × 25 mm area, and subjected to a tensile test with a rate of 1 mm/min. The results were compared by plotting the stress versus strain multigraphs. For this test, five specimens for each sample were used.

3.8. SEM Analysis of the Wood Substrate after Performing the Tensile Test. After displacement of the bonded wood substrates, SEM analysis was employed to analyze the bonded area. The micrographs were acquired with a Nova NanoSEM 630 scanning electron microscope (FEI Company, Hillsboro, OR, USA) at an acceleration voltage of 10 kV. All specimens were sputtered with a thin layer of conductive metal (Au) to prevent the charging of the samples during SEM analysis.

3.9. Simulation Analysis of the Polyurethane Adhesive Formulations. A tensile test modeling was performed using LS-DYNA, specialized software for simulating nonlinear transient phenomena. The test conditions were conducted in accordance with EN ISO 1421, Method 1, called the Strip Test, which uses strip-type specimens and is used to determine the tensile strength and elongation at break.

Since the specimen geometry is relatively simple, the modeling was carried out in three dimensions using a structured hexahedral mesh, as shown in Scheme 2, with SOLID 3 type elements, which are fully integrated quadratic 8 node elements with nodal rotations.

Mesh characteristics are presented in Table 2.

To comply with the testing conditions, two sets of nodes were defined on both pieces of wood, with a distance of 200 mm between the two sets, representing the actual clamping distance between the grips. The right piece of wood is fixed using the corresponding set of nodes by applying a boundary condition that locks these nodes, while the other piece of wood is subjected to a constant pulling speed of 1 mm/min through the corresponding set of nodes.

https://doi.org/10.1021/acsomega.3c04393
ACS Omega 2023, 8, 38178−38190

Scheme 2. Simulated Model of the Specimens: 1—Adhesive; 2—Mobile Wood Strip; 3—Fixed Wood Strip

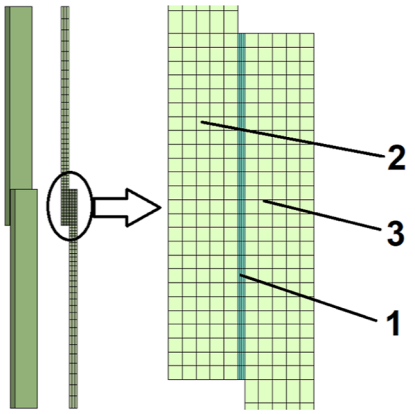

Table 2. Mesh Characteristics

nodes	elements	parts	materials	sections
15,750	13,000	3	2	1

To validate the virtual model, the displacement and force were recorded as a function of time. Subsequently, the force–displacement curve obtained from the model was compared with the experimental one.

The material properties used into the program for modeling the conducted test correspond to the plastic-kinematic (a) and elastic material models (b), as described below:

3.9.1. Plastic Kinematic Material Model. To model the adhesive used between the two pieces of wood, the plastic-kinematic material model was utilized. The plastic-kinematic material model simulates isotropic and kinematic hardening plasticity, with an option to include the effects due to the rate of deformation. The rate of deformation is calculated using the Cowper–Symonds model,[25] which scales the yield stress by a factor

$$\sigma_y = \left[1 + \left(\frac{\dot{\varepsilon}}{C}\right)^{1/p}(\sigma_0 + \beta \cdot E_p \cdot \varepsilon_p^{\text{eff}})\right] \quad (1)$$

$$E_p = \frac{E_{\tan} \cdot E}{E - E_{\tan}} \quad (2)$$

where σ_0—initial yield stress; $\dot{\varepsilon}$—the strain rate; C and P—the Cowper–Symonds strain rate parameters; β—the strain hardening parameter (adjusts the contribution of isotropic and kinematic hardening); $\varepsilon_p^{\text{eff}}$—the effective plastic strain; E_p—the plastic hardening modulus, which is given in terms of the elastic modulus E; $E_{\tan}$—the tangent of the elastic modulus.[25]

Alternatively, a fully viscoelastic formulation incorporating the Cowper–Symonds formulation on the yield surface is optional. Kinematic, isotropic, or a combination of kinematic and isotropic hardening can be specified by varying the parameter β (hardening coefficient) between 0 and 1.

Table 3 presents the material constants used in the proposed simulation[26]

3.9.2. Elastic Material Model. Since the test is conducted at a low speed in the quasi-static domain, the two pieces of wood are modeled using the elastic material model described by eq 3. For the linear elastic material model, the constitutive equations are given by the generalized Hooke's law[27]

$$\varepsilon_x = \frac{1}{E}(\sigma_x - \nu(\sigma_y + \sigma_z))$$

$$\varepsilon_y = \frac{1}{E}(\sigma_y - \nu(\sigma_x + \sigma_z))$$

$$\varepsilon_z = \frac{1}{E}(\sigma_z - \nu(\sigma_x + \sigma_y))$$

$$\gamma_{xy} = \frac{1}{G}\tau_{xy}$$

$$\gamma_{yz} = \frac{1}{G}\tau_{yz}$$

$$\gamma_{zx} = \frac{1}{G}\tau_{zx} \quad (3)$$

where

$$\{\sigma\} = \begin{Bmatrix} \sigma_x(x, y, z, t) \\ \sigma_y(x, y, z, t) \\ \sigma_z(x, y, z, t) \\ \tau_{xy}(x, y, z, t) \\ \tau_{yz}(x, y, z, t) \\ \tau_{zx}(x, y, z, t) \end{Bmatrix} \text{—stress components}$$

$$\{\varepsilon\} = \begin{Bmatrix} \varepsilon_x \\ \varepsilon_y \\ \varepsilon_z \\ \gamma_{xy} \\ \gamma_{yz} \\ \gamma_{zx} \end{Bmatrix} \text{—strain components}$$

E—Young's modulus. G—Shear modulus. ν—Poisson's ratio.

There is a dependency relationship between the three parameters

$$G = \frac{E}{2(1 + \nu)}$$

In LS-DYNA software, it is used an isotropic hypoelastic material[28] which is available for beam, shell, and solid elements. The axial and bending damping factors are used to damp down numerical noise. The update of the force resultants, F_i, and moment resultants, M_i, includes the damping factors

Table 3. Plastic-Kinematic Material Constants Used[26]

nr. crt	component	material	ρ (Adhesive density, kg/m^3)	E (module of elasticity, MPa)	ν (Poisson's coefficient)	σ_y (tension at flow)	$E_{\tan}$
1	adhesive	psolyurethane	1,0	2	0,35	1	0

https://doi.org/10.1021/acsomega.3c04393
ACS Omega 2023, 8, 38178−38190

Table 4. Constants Used for the Elastic Material[29]

component	material	ρ (wood density, kg/m^3)	E (module of elasticity, MPa)	ν (Poisson's coefficient)
wood strips	F. sylvatica L.	672	12.1×10^3	0, 37

$$F_i^{n+1} = F_i^n + \left(1 + \frac{DA}{\Delta t}\right)\cdot \Delta F_i^{n+1/2} \quad (4)$$

$$M_i^{n+1} = M_i^n + \left(1 + \frac{DB}{\Delta t}\right)\cdot \Delta M_i^{n+1/2} \quad (5)$$

In Table 4, the material constants for the two pieces of wood (*F. sylvatica* L.) are given presented.[29]

4. RESULTS AND DISCUSSION

4.1. Determination of the Hydroxyl Index of Pol-L. The first step of our study involved the determination of the hydroxyl number for the glycolysis product, Pol-L based on the standard method ASTM D4274-99-method A (detailed in Section 3.1). Thus, the hydroxyl number for the glycolysis product was 466.9 mg KOH/g. This information was useful to develop polyurethane adhesive formulations based on the reaction of Pol-L-bio-based polyol (component A) and diisocyanate curing agent (component B), as detailed in Section 2.2.2.

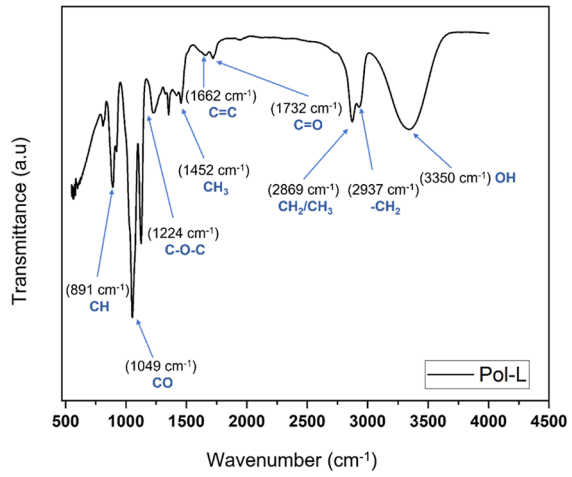

Figure 1. FT-IR analysis of the Pol-L glycolysis product resulted after the depolymerization of lignocellulose broadleaf biomass.

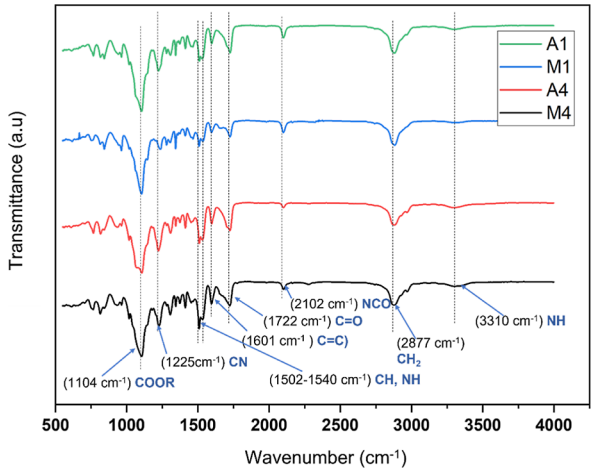

Figure 2. FT-IR analysis of blank (M1 and M4) and Pol-L-based polyurethane adhesive formulations (A1 and A4).

4.2. FT-IR Analysis of the Pol-L Glycolysis Product and Polyurethane Adhesives. Pol-L bio-oil was characterized by FT-IR analysis to evidence the degradation components that resulted after the depolymerization of the lignocellulose-based biomass. Thus, in Figure 1, the FT-IR spectrum of the glycolysis product is presented.

The intense signal registered at 3350 cm^{-1} corresponds to OH groups, while the peaks from 2937 to 2869 cm^{-1} were assigned to $-CH_2$ and CH_3 vibration stretching.[21] The peak from 1732 cm^{-1} was identified as C═O groups assigned to the aldehydes, ketones, and ester groups from the compounds resulted from the glycolysis of lignocellulose material.[21,30] The stretching vibration of C═C groups from 1662 cm^{-1} was assigned to the aromatic ring from the lignin structure. At 1224 cm^{-1}, a characteristic band was attributed to the ether C−O−C groups bending from the initial structure of lignin, while at 1049 cm^{-1}, the CO group is associated with the breaking of glucoside bonds from the cellulose structure.[30]

To prove the reaction between the two main components and the formation of urethane groups, FT-IR analysis was performed for the most relevant blank and Pol-L-based polyol adhesive formulations. In Figure 2, the FT-IR spectra of blank samples M1 and M4, respectively, of the bio-based polyurethane adhesives A1 and A4 registered the characteristic peaks for the urethane group.

The signal from 3310 cm^{-1} was attributed to NH stretching, while the signal from 1722 cm^{-1} was assigned to C═O stretching, confirming the formation of urethane groups as a result of the reaction between the OH groups from component A and NCO groups from MDI (component B).[31] Vibrations of CH_2 groups were registered at 2877 cm^{-1}. The NCO signal from 2102 cm^{-1} was assigned to the terminal groups of the polymeric chain. The C═C registered at 1601 cm^{-1} was attributed to the aromatic rings of the MDI or to the aromatic components resulted after the depolymerization of the lignin structure.[32,33] The signal from 1502 to 1540 cm^{-1} was assigned to the N−H vibration in the plane of the amide group.[33] Another indication that the reaction took place was proved by the C−N stretching vibrations in amine assigned at 1225 cm^{-1}.[33,34]

4.3. TGA Analysis of Pol-L Glycolysis Product, Blank Samples M1, M4, and Adhesives A1, A4. In Figure 3, TGA analyses give information on the thermal stability of the most relevant products. For Pol-L bio-polyol, the highest mass loss is registered around 200−210 °C, which can be attributed to the boiling point of DEG solvent (approx. 240 °C).

The blank samples M1 and M4 registered the highest mass loss in the 300−400 °C temperature range. The main difference between the two blank samples is determined by the crosslinking density, which is higher for the M1 formulation. This is due to a higher amount of trifunctional commercial polyether-polyol PETOL 46-3MB detectable by the higher amount of residue and registered in Figure 3A (blue line compared with black line). Similar behavior was registered for A1 and A4 formulations, with A1 being more stable after

https://doi.org/10.1021/acsomega.3c04393
ACS Omega 2023, 8, 38178−38190

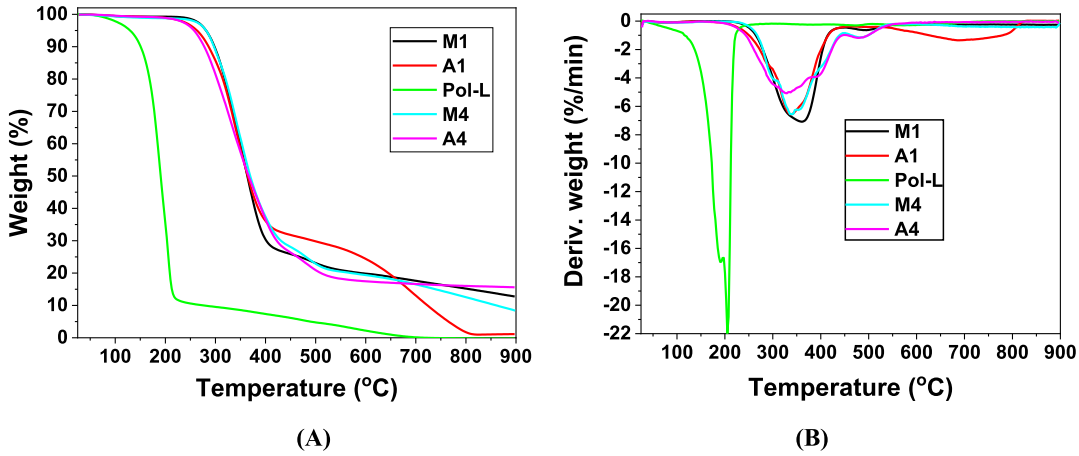

(A) (B)

Figure 3. TGA (A) and DTA (B) analysis of the Pol-L glycolysis, polyurethane blank samples M1, M4, and adhesives A1 and A4.

Scheme 3. Schematic Determination of Pot-Life/Working Time of the Polyurethane Adhesive Formulations (1—Data Acquisition; 2—FLIR Camera; 3—Mixture Stirring)

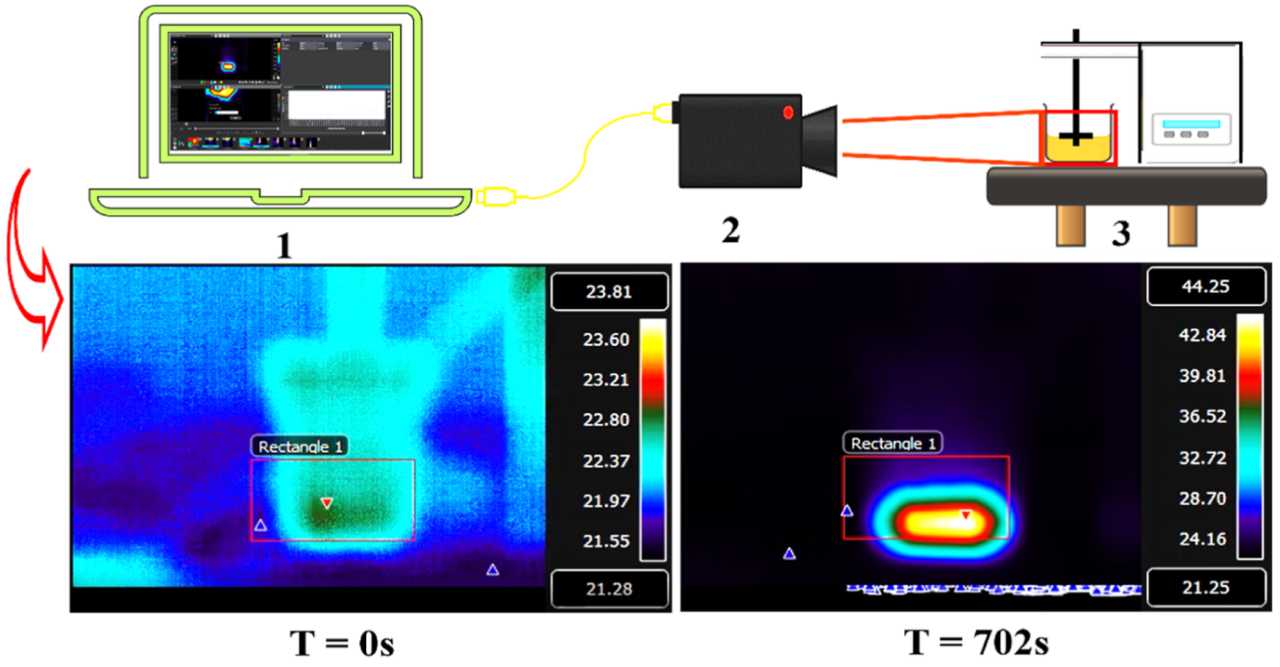

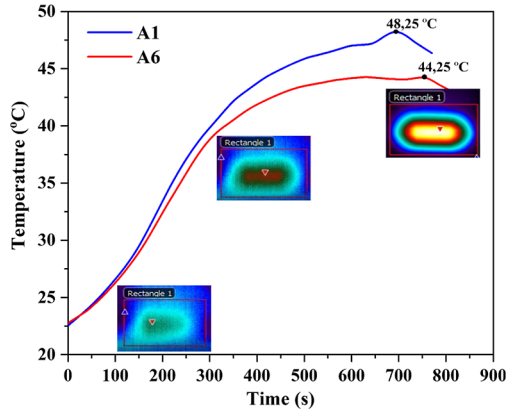

Figure 4. Temperature versus time during continuous stirring of the bicomponent polyurethane adhesive formulation.

Table 5. T_g Values for Bio-Based PUR Adhesives and Their Counterparts

sample	T_g (°C)	sample	T_g (°C)
M1	80	A1	73
M2	57	A2	69
M3	65	A3	60
M4	56	A4	63
M5	55	A5	63
M6	50	A6	58

450 °C compared with A4 considering the higher amount of PETOL 46-3MB commercial compound used in this case.

In the case of bio-based polyurethane adhesive A1, additional mass loss was registered in the 600−700 °C temperature range compared with its M1 counterpart, which was attributed to the higher thermal sensitivity of the polyurethane chains from the bio-polyol glycolysis product. However, in the case of A4, this behavior was different, with

https://doi.org/10.1021/acsomega.3c04393
ACS Omega 2023, 8, 38178−38190

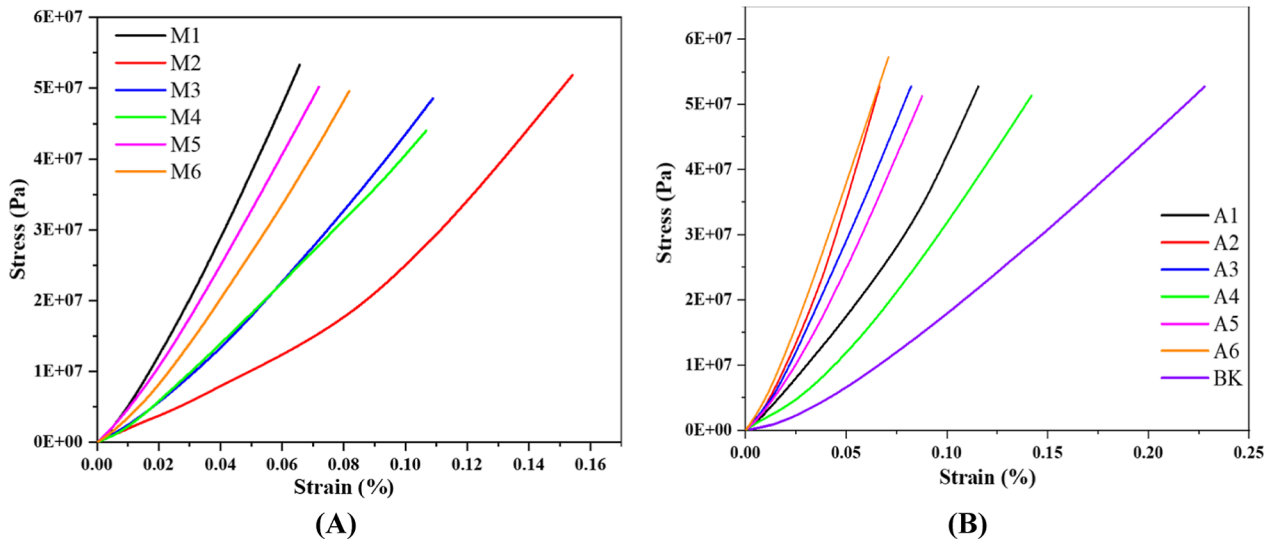

Figure 5. Stress versus strain registered for blank (A), and Pol-L-based PUR adhesive formulations (B).

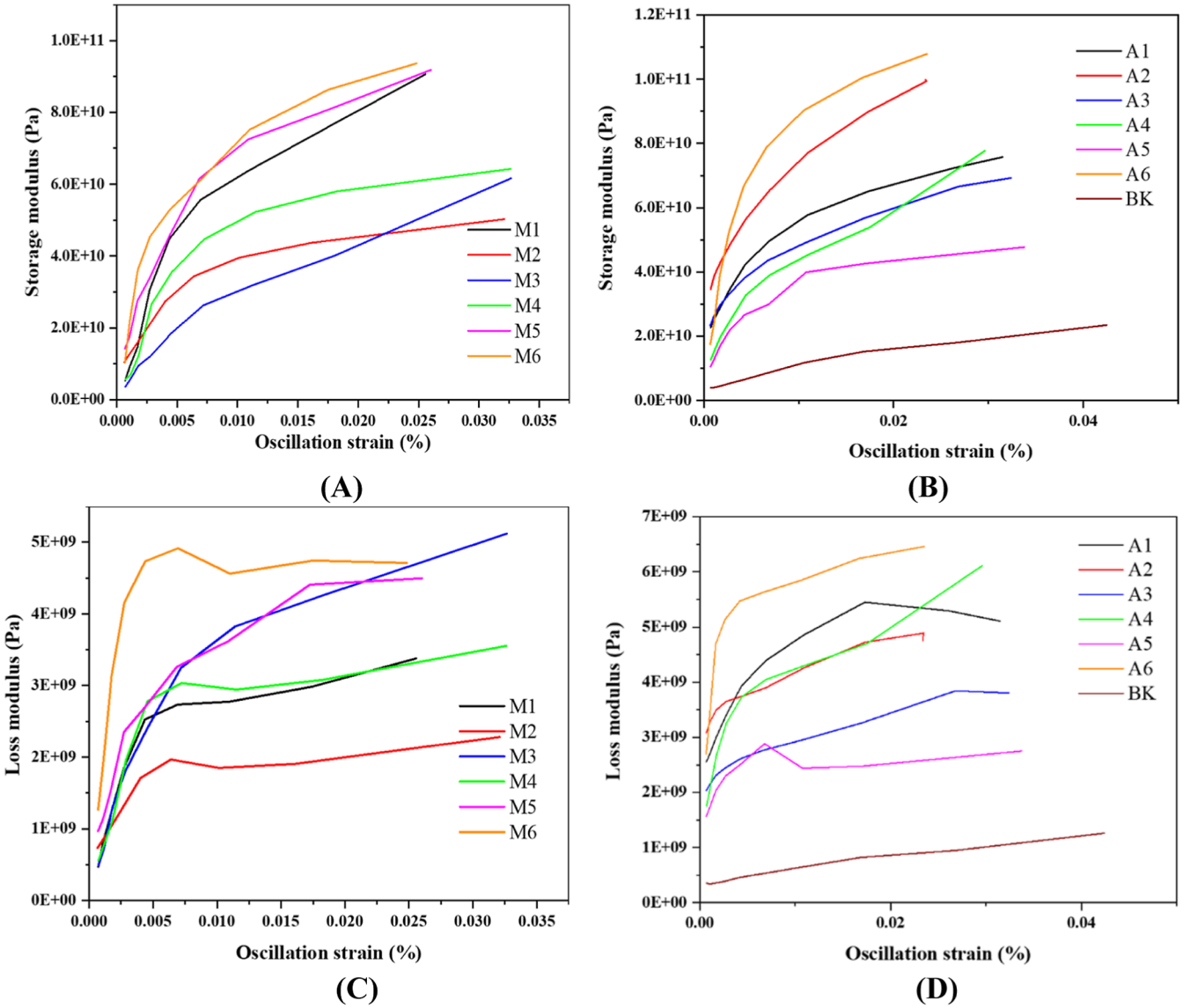

Figure 6. Three-point bending test in oscillation mode—registration of storage and loss modulus for blank samples (A, C) and for Pol-L-based PUR adhesives (B, D).

https://doi.org/10.1021/acsomega.3c04393
ACS Omega 2023, 8, 38178−38190

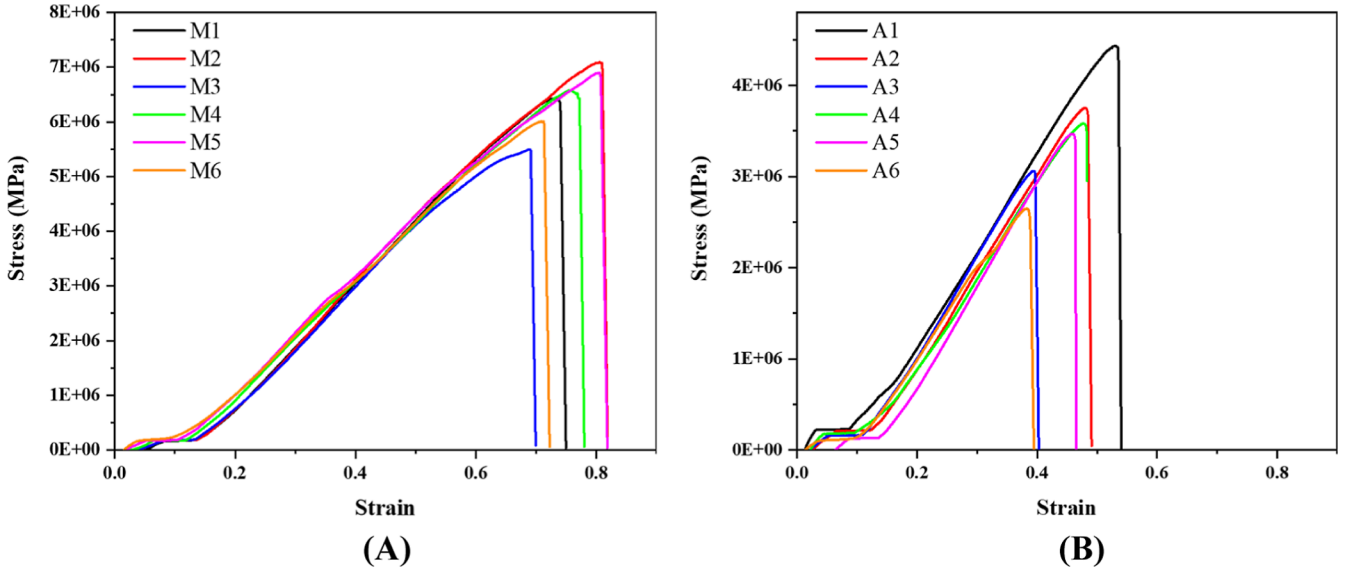

Figure 7. Tensile tests of the blank (A) and Pol-L-based PUR adhesives (B).

Table 6. Values of Maximal Failure Stress and Failure Strain for All PUR Adhesive Specimens

sample	failure stress (MPa)	failure strain	sample	failure Stress (MPa)	Failure strain	MDI, %
M1	6.4 ± 0.20	0.7 ± 0.020	**A1**	4.4 ± 0.16	0.53 ± 0.014	45.9
M2	7 ± 0.15	0.8 ± 0.013	**A2**	3.7 ± 0.18	0.48 ± 0.011	44.4
M3	5.5 ± 0.12	0.68 ± 0.021	**A3**	3.1 ± 0.23	0.39 ± 0.016	42.8
M4	6.5 ± 0.21	0.76 ± 0.016	**A4**	3.6 ± 0.19	0.47 ± 0.015	45.9
M5	6.8 ± 0.10	0.8 ± 0.13	**A5**	3.5 ± 0.12	0.45 ± 0.010	44.4
M6	6 ± 0.17	0.71 ± 0.014	**A6**	2.6 ± 0.11	0.38 ± 0.017	42.8

Scheme 4. Successive Data Obtained from Numerical Simulation

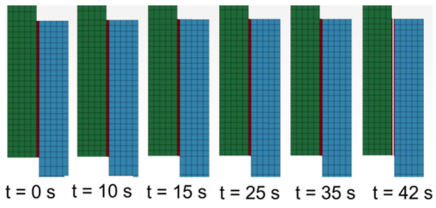

the mass loss being lower compared to the M1 counterpart. It is worth mentioning that the A4 formation had the highest thermal stability after 700 °C compared with all other PUR samples analyzed by TGA.

4.4. Determination of Pot-Life/Working Time of the Pol-L-Based Polyurethane Adhesive Formulations. The pot life or the working time is specific for the bi-component formulations and measures the average length of time between the start of mixing and the moment of application. During this time interval, the adhesive retains a low enough viscosity that allows application on the selected support. After this time, the adhesive may set before the parts are assembled. To determine the pot-life in an accurate manner, an innovative set-up is described in Scheme 3. During the mixing of the polyurethane bio-based formulations, an infrared camera (Scheme 3—number 2) was positioned close to the reaction vessel (Scheme 3—number 3). The temperature increase was monitored in time while keeping the mixing rate constant, the data being collected by a data acquisition system (Scheme 3—number 1).

In Figure 4, the temperature was plotted versus time, and the highest temperature of 48.25 °C was registered after 700 s for adhesive A1, which had the largest amounts of trifunctional commercial polyol and diisocyanate compound. For the other relevant formulation, A6 (in which the lowest amounts of trifunctional commercial polyol and MDI were used), the reaction temperature of 44.25 °C was collected after 800 s.

It is worth mentioning that the temperature rises more abruptly after 100 s, as shown in Figure 4. Considering this period as the optimum time for mixing the whole components, the adhesives can be applied in a range of maximum 600 to 700 s (10 to 11 min), depending on the bio-based formulation, while keeping the speed of stirring at 150 rpm.

4.5. DMA Analysis of the Polyurethane Adhesive Formulations. DMA analysis was performed for all 6 bio-based PUR adhesive formulations and their blank counterparts to determine the T_g values (Table 5). The glass transition temperature (T_g) corresponds to the maximum of the tangent(delta) values from the Tan(delta)-temperature plots[35] presented in Figure S1E,F in the Supporting Information. In Figure S1A, the storage modulus for the M1−M6 blank specimens is higher compared with the loss modulus (Figure S1C), suggesting a rigid structure. Similar behavior was observed in the case of the bio-based adhesives that registered lower values of their loss modulus compared to their storage modulus (Figure S1D compared to Figure S1B).

The T_g value of A4−A6 is higher compared with the values registered for their blank counterparts, indicating a stiffer structure of these formulations (Table 5). The same behavior was registered for A2 (a T_g value of 69 °C compared to 57 °C of the M1 sample). Thus, the bio-based glycolysis product improved the stiffness of the bicomponent PUR formulations

https://doi.org/10.1021/acsomega.3c04393
ACS Omega 2023, 8, 38178−38190

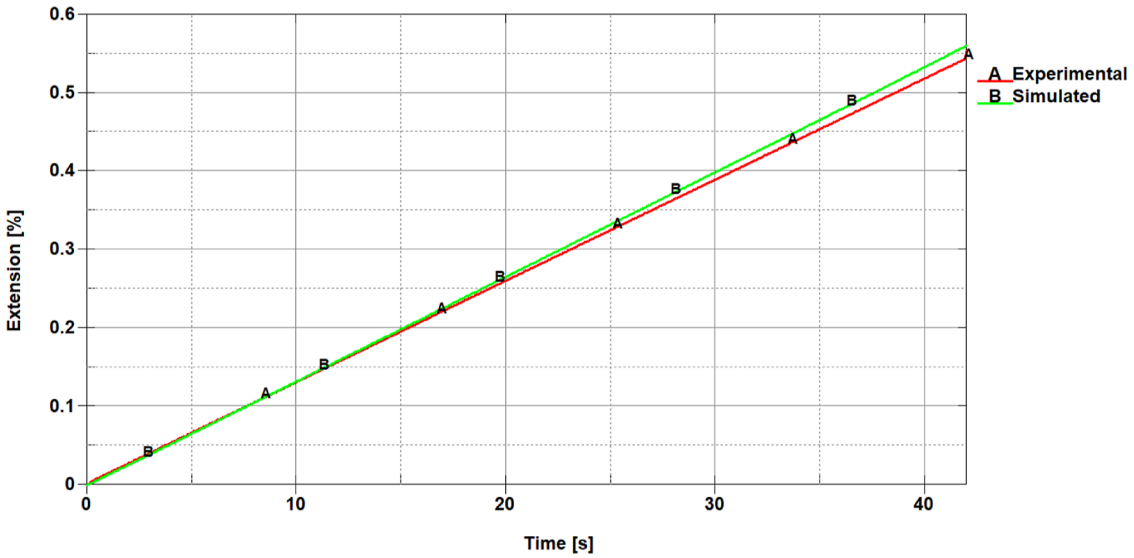

Figure 8. Extension versus time experimental and simulated data.

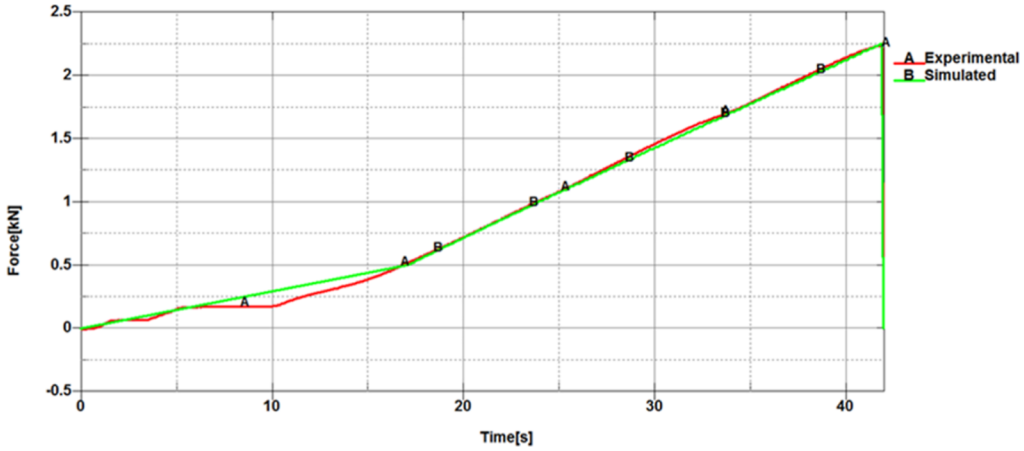

Figure 9. Force versus time experimental and simulated data.

in the case of A2, A4, A5, and A6 adhesives compared to their blanks (Table 5).

4.6. Three-Point Bending Test of the Polyurethane Adhesive Formulations. *4.6.1. Stress versus Strain.* One of the most used test methods for determining the shearing strength of wood-adhesive-wood sandwich structure is the three-point bend test (3PBT), often known as the short beam shear test.[36] The purpose of this test was to study the bonding in a sandwich structure of wood-bio-based adhesive-wood. Figure 5 illustrates comparative stress−strain plots for polyurethane adhesives (A1 ÷ A6) (Figure 5B) and their blank counterparts (M1 ÷ M6) (Figure 5A) obtained via 3PBT. It is worth mentioning that the samples did not break; the analysis was performed until reaching the maximal load allowed by the instrument.

As can be observed from Figure 5B, the presence of the adhesives in all the sandwich structures ensured their higher flexural strength compared to BK (wood substrates without adhesive). The higher increase in strength for some adhesive formulations could be ascribed to the distinct molar ratios between their components.

In terms of flexural deformation, these results offered evidence of the lower tendency of these materials to bend when a force was applied compared to BK. The ratio of stress to strain can offer information on the flexural modulus (also known as the bending modulus). A material that is more resistant to the same bending stress applied indicates a higher flexural modulus. In our case, samples A6, A2, A3, and A5 displayed the higher bending resistance, while samples A1 and A4 indicated higher flexibility of these sandwich structures. 3PBT for blank counterparts M1, M5, and M6 indicated that these samples also possess a higher stiffness. By comparing A2, A4, A5, and A6 with their blanks (M2, M4, M5, and M6), a higher mechanical performance in terms of stress is observed, which is in good agreement with the T_g values obtained previously.

4.6.2. Oscillation Mode. 3PBT was also performed in oscillation mode to evaluate the storage and the loss modulus of the same sandwich structures by varying the amplitude with a constant frequency (1 Hz). Usually, when storage modulus values are higher than loss modulus values, this indicates the presence of crosslinking sites inside the analyzed polymeric material. All samples exhibited this behavior, confirming the crosslinked nature of the bio-based adhesive, except BK (the wood substrate), which had no adhesive (Figure 6). Samples A6, A2 or M6, M5, and M1 displayed higher storage modulus

https://doi.org/10.1021/acsomega.3c04393
ACS Omega 2023, 8, 38178−38190

values, indicating a higher capacity of storing the energy as oscillation strain increased, while A3, A5 or M4, and M2 displayed lower storage modulus values. Furthermore, when comparing Figure 6A,B, it can be observed that some of the bio-based formulations displayed a higher flexural strength than their analogous blank counterparts (except formulations A3 and A5 compared with M3 and M5).

4.7. Mechanical Tensile Tests of the Polyurethane Adhesive Formulations. Further, a tensile test was performed on adhesively bonded single-lap joint samples to obtain complementary data on the mechanical properties of the bio-based formulations employed. The results obtained are comparatively summarized in Figure 7. One averaged curve of five specimens tested was plotted for each type of bio-based adhesive formulation.

As can be observed from Figure 7A,B, the uniaxial tensile stress−strain plots of the bio-based adhesives and their blank counterparts exhibited non-linear behavior.[37]

From the stress−strain curves, the tensile test at break and the failure strain were analyzed, and the data indexed in Table 6 indicates the variation of the failure stress dependent on the amount of MDI in the adhesive formulations which are comparable with literature examples for different polymer composites[38−41] and polyurethane adhesives.[42−44]

Thus, in Table 6, the maximal values of failure stress indicate that at lower amounts of MDI (expressed as weight percentage), the failure stress decreases in both series of M1 ÷ M6 and A1 ÷ A6, probably due to lower crosslinking sites in the PUR formulation. Nevertheless, the deformation pattern follows similar trends for all the tested samples. Among all the adhesive formulations, higher strength and slightly higher plastic deformation capability were observed for the M1 ÷ M6 series but also for A1, A2, A4, or A5. In the case of the A1 ÷ A6 series, both the adhesive strength and the strain values obtained are slightly lower compared with their blanks, probably due to the unreacted DEG from the glycolysis product, which induces a plasticizing effect on the resulting crosslinked polymeric structure of the bio-based adhesives.

Yet, the bio-based adhesive strength is still high enough to ensure an efficient bond between the two wood strips.[45,46] Moreover, the slight plasticity of these bio-based adhesives may help reduce the brittleness of the adhesive joint, thus maintaining the wood strips in contact for a longer time when loading is applied on the sandwich structure wood-adhesive-wood.[47−49]

4.8. Post-Fracture Investigation after Tensile Tests by SEM Analysis. In Figure S2, SEM micrographs were collected for the wood substrate and the area on which the blank and Pol-L-based PUR adhesive were applied after the tensile test was performed. Usually, the adhesive bonding is analyzed after the displacement of the bonded structures to study the propagation of the rupture upon applied stress at the macroscopic level. According to literature data, there are three possible types of adhesive bond failure that can occur during the tensile test:[50,51] (i) the adhesive is on both surfaces after detachment of the bonded strips (cohesive failure), (ii) the adhesive remains only on one of the surfaces (adhesive failure or delamination), and (iii) the substrate is broken due to adhesive bonding strength (substrate or adherent failure).[52]

The desirable sort of failure is one in which the adhesion between two adherends or within the adhesive itself indicates that the bonded materials have achieved their maximal strength.[50]

In our case, there were no obvious changes after the tensile test in the bonded area observable at the macroscopic level. Thus, to give some information about the type of adhesive failure for the bio-based PUR adhesives, SEM analysis was performed for the wood strip, the adhesive layer for blank, and the Pol-L-based formulations (Figure S2). Since all the samples had similar behavior, in Figure S2b and Figure S2c, the microstructure of the specimens is presented for M6, respectively A6 formulations.

Comparing the unbonded wood substrate (Figure S2a) with the other two specimens (Figure S2b and Figure S2c) it was noticed that the adhesive layer is still present on the surface and there are no splinters of wood detached from the surface for both specimens (blank and bio-based adhesive). The adhesive layer was continuous on the surface of the wood substrate, revealing a complete protrusion of the adhesive in the interstitials of the wood structures, which indicates a good interaction between the adhesive and substrate.[53] Furthermore, the adhesive layer had no cracks but a slightly porous aspect on the wood surface (yellow circles in Figure S2b,c). According to the SEM investigation, the PUR adhesive layer developed few striations (marked with yellow arrows in Figure S2) on the uniaxial direction of the applied stress, indicating a cohesive failure. Additionally, the striations of the layer indicate that the adhesive material had an elastic component followed by a slight brittle/rigid behavior attributed to the pores from the adhesive layer.[53,54]

4.9. Simulation Analysis of the Polyurethane Adhesive Formulations. A numerical simulation of the adhesive bonding tests on two pieces of wood was conducted, following the EN ISO 1421 method 1 standard. The obtained results are presented in the following figures, highlighting both the adhesive's stretching behavior and its failure during the test.

In Scheme 4, successive data obtained from numerical simulation was obtained as a correlation between time and deformation to final displacement of the wood substrates. During the tensile test, the right wood strip is fixed while the other is pulled with a tension of 1 mm/min. As shown in Scheme 4, at the beginning of the motion, both parts move together due to the elasticity of the wood, while after a duration of 15 s, the adhesive starts to deform. After 42 s, the complete breaking of the two wood strips occurs.

This is in good correlation with the tensile test and the SEM analysis that indicated both elastic and brittle behavior of the wood-adhesive-wood material.

In Figure 8, the experimentally recorded extension exhibited a very accurate correlation between simulated and experimental data.

In Figure 9, the experimentally recorded force exhibits a plateau-like variation in the initial test phase until around 17 s, which is different from the variation observed from 17 to 42 s. This difference is not reflected in the relative displacement graph, which can be attributed to the compliance of the testing machine. However, the material models used, although relatively simple in formulation, provided a good approximation of the experimental data with errors below 5%.

5. CONCLUSIONS

In conclusion, bio-polyol products were obtained by the depolymerization of lignocellulose broadleaf sawdust through an acid catalysis solvolysis reaction in the presence of DEG. The bio-oil resulted from the reaction was used to formulate 6 bicomponent PUR adhesives.

https://doi.org/10.1021/acsomega.3c04393
ACS Omega 2023, 8, 38178−38190

The adhesive films were characterized by FT-IR, TGA, and DMA, while the mechanical performances were investigated by tensile and 3PBT tests.

An innovative method applied for the determination of the working time indicated a 10 to 12 min pot life for the bio-based adhesives.

The bio-based component increased the T_g value and enhanced the stiffness of the bicomponent PUR formulations, as demonstrated by the 3PBT tests performed in two modes (stress vs strain and oscillation mode). The unidirectional tensile tests showed that the slight plasticity of the bio-based adhesives could decrease the brittleness of the wood-adhesive-wood material.

The post-fracture SEM investigations indicated a cohesive failure for all formulations and an elastic component, followed by a slight brittle/rigid behavior after detachment of the wood strips. The numerical simulation performed in LS-DYNA of the adhesive bonding tests exhibited an accurate correlation between simulated and experimental data for both extension and force.

■ ASSOCIATED CONTENT

Supporting Information

The Supporting Information is available free of charge at https://pubs.acs.org/doi/10.1021/acsomega.3c04393.

Determination of hydroxyl index of Pol-L glycolysis product; storage modulus, loss modulus, and Tan(delta) in the temperature range −30 ÷150 °C for M1−M6, respectively, A1−A6 PUR adhesives; and SEM micrographs of the unbonded wood substrate, the bonded area bonded with blank, and Pol-L-based PUR adhesives after the tensile test (PDF)

■ AUTHOR INFORMATION

Corresponding Author

Alexandra Mocanu − *Faculty of Chemical Engineering and Biotechnologies, University Politehnica of Bucharest, 011061 Bucharest, Romania; National Institute for Research and Development in Microtechnologies—IMT Bucharest, 077190 Bucharest, Romania;* orcid.org/0000-0003-0469-9974; Email: alexandra.mocanu@upb.ro

Authors

Edina Rusen − *Faculty of Chemical Engineering and Biotechnologies, University Politehnica of Bucharest, 011061 Bucharest, Romania;* orcid.org/0000-0002-1660-017X

Gabriela Toader − *Military Technical Academy "Ferdinand I", 050141 Bucharest, Romania*

Aurel Diacon − *Faculty of Chemical Engineering and Biotechnologies, University Politehnica of Bucharest, 011061 Bucharest, Romania; Military Technical Academy "Ferdinand I", 050141 Bucharest, Romania;* orcid.org/0000-0001-5171-2049

Florin Marian Dîrloman − *Military Technical Academy "Ferdinand I", 050141 Bucharest, Romania*

Liviu Cristian Matache − *Military Technical Academy "Ferdinand I", 050141 Bucharest, Romania*

Florentina Alexe − *Research and Innovation Center for CBRN Defense and Ecology, 041327 Bucharest, Romania*

Adrian Dinescu − *National Institute for Research and Development in Microtechnologies—IMT Bucharest, 077190 Bucharest, Romania*

Complete contact information is available at: https://pubs.acs.org/10.1021/acsomega.3c04393

Notes

The authors declare no competing financial interest.

■ ACKNOWLEDGMENTS

The authors acknowledge the financial support received from the Competitiveness Operational Program 2014−2020 Priority axis: research, technological development, and innovation (RDI) in support of economic competitiveness and business development—Project: "Greenol-Biopolyols obtained through an unconventional technology of vegetal waste recovery" Project code: 122990. The mechanical investigations were supported by the Ministry of Research, Innovation, and Digitalization (UEFISCDI) through PN-III-P2-2.1-PTE-2021—contract no. 80PTE/2022 and 105PTE/2022. This publication is based on work from COST Action CA18120 (CERTBOND—"Reliable roadmap for certification of bonded primary structures" https://certbond.eu/), supported by COST (European Cooperation in Science and Technology). The publication fee is financially supported by the University Politehnica of Bucharest within the PubArt Program.

■ REFERENCES

(1) *The Editors of Encyclopaedia Britannica*; Encyclopedia Britannica, 28 May 2023 (updated).

(2) Butnaru, E.; Pamfil, D.; Stoleru, E.; Brebu, M. Characterization of bark, needles and cones from silver fir (Abies alba mill.) towards valorization of biomass forestry residues. *Biomass Bioenergy* **2022**, *159*, 106413.

(3) Semaan, J.-N.; Belandria, V.; Missaoui, A.; Sarh, B.; Gökalp, I.; Bostyn, S. Energy analysis of olive pomace valorization via hydrothermal carbonization. *Biomass Bioenergy* **2022**, *165*, 106590.

(4) Fernando-Foncillas, C.; Varrone, C. Potential of the sewage sludge valorization in Scandinavia by co-digestion with other organic wastes: A techno-economic assessment. *J. Cleaner Prod.* **2021**, *324*, 129239.

(5) Panopoulos, K.; Kardaras, G.; Kraia, T.; Bampaou, M. Chapter 5 - Environmental assessment of biomass thermochemical conversion routes through a life cycle perspective. In *Environmental Assessment of Renewable Energy Conversion Technologies*; Fokaides, P. A., Kylili, A., Georgali, P.-z., Eds.; Elsevier, 2022; pp 85−128.

(6) deLlano-Paz, F.; Martínez Fernandez, P.; Soares, I. Addressing 2030 EU policy framework for energy and climate: Cost, risk and energy security issues. *Energy* **2016**, *115*, 1347−1360.

(7) Sikkema, R.; Proskurina, S.; Banja, M.; Vakkilainen, E. How can solid biomass contribute to the EU's renewable energy targets in 2020, 2030 and what are the GHG drivers and safeguards in energy- and forestry sectors? *Renewable Energy* **2021**, *165*, 758−772.

(8) Watanabe, M. D. B.; Cherubini, F.; Tisserant, A.; Cavalett, O. Drop-in and hydrogen-based biofuels for maritime transport: Country-based assessment of climate change impacts in Europe up to 2050. *Energy Convers. Manage.* **2022**, *273*, 116403.

(9) Carregosa, I. S. C.; Carregosa, J. d. C.; Silva, W. R.; Santos, T. M.; Wisniewski Jr, A. Thermochemical conversion of aquatic weed biomass in a rotary kiln reactor for production of bio-based derivatives. *J. Anal. Appl. Pyrolysis* **2023**, *173*, 106048.

(10) Pesante, G.; Frison, N. Recovery of bio-based products from PHA-rich biomass obtained from biowaste: A review. *Bioresour. Technol. Rep.* **2023**, *21*, 101345.

(11) Hoang, A. T.; Nižetić, S.; Ong, H. C.; Mofijur, M.; Ahmed, S. F.; Ashok, B.; Bui, V. T. V.; Chau, M. Q. Insight into the recent advances of microwave pretreatment technologies for the conversion of lignocellulosic biomass into sustainable biofuel. *Chemosphere* **2021**, *281*, 130878.

(12) Zhou, N.; Yang, J.; Lu, X.; Xin, Z.; Xu, C.; He, Q. Microwave-assisted depolymerization of lignin and a biphasic extraction method for the recovery of bio-oil and phenolic monomers. *J. Anal. Appl. Pyrolysis* **2022**, *161*, 105403.
(13) Usmani, Z.; Sharma, M.; Awasthi, A. K.; Lukk, T.; Tuohy, M. G.; Gong, L.; Nguyen-Tri, P.; Goddard, A. D.; Bill, R. M.; Nayak, S. C.; Gupta, V. K. Lignocellulosic biorefineries: The current state of challenges and strategies for efficient commercialization. *Renewable Sustainable Energy Rev.* **2021**, *148*, 111258.
(14) Nguyen, B. H.; Perkins, R. J.; Smith, J. A.; Moeller, K. D. Solvolysis, Electrochemistry, and Development of Synthetic Building Blocks from Sawdust. *J. Org. Chem.* **2015**, *80*, 11953−11962.
(15) Ang, A. F.; Ashaari, Z.; Lee, S. H.; Md Tahir, P.; Halis, R. Lignin-based copolymer adhesives for composite wood panels − A review. *Int. J. Adhes. Adhes.* **2019**, *95*, 102408.
(16) Gao, C.; Li, M.; Zhu, C.; Hu, Y.; Shen, T.; Li, M.; Ji, X.; Lyu, G.; Zhuang, W. One-pot depolymerization, demethylation and phenolation of lignin catalyzed by HBr under microwave irradiation for phenolic foam preparation. *Composites, Part B* **2021**, *205*, 108530.
(17) Sreejaya, M. M.; Jeevan Sankar, R.; K, R.; Pillai, N. P.; Ramkumar, K.; Anuvinda, P.; Meenakshi, V. S.; Sadanandan, S. Lignin-based organic coatings and their applications: A review. *Mater. Today: Proc.* **2022**, *60*, 494−501.
(18) Kim, J.-Y.; Lee, H. W.; Lee, S. M.; Jae, J.; Park, Y.-K. Overview of the recent advances in lignocellulose liquefaction for producing biofuels, bio-based materials and chemicals. *Bioresour. Technol.* **2019**, *279*, 373−384.
(19) Hosseinpourpia, R.; Eceiza, A.; Adamopoulos, S. Polyurethane Wood Adhesives Prepared from Modified Polysaccharides. *Polymers* **2022**, *14*, 539.
(20) Hussin, M. H.; Abd Latif, N. H.; Hamidon, T. S.; Idris, N. N.; Hashim, R.; Appaturi, J. N.; Brosse, N.; Ziegler-Devin, I.; Chrusiel, L.; Fatriasari, W.; Syamani, F. A.; Iswanto, A. H.; Hua, L. S.; Al Edrus, S. S. A. O.; Lum, W. C.; Antov, P.; Savov, V.; Rahandi Lubis, M. A.; Kristak, L.; Reh, R.; Sedliačik, J. Latest advancements in high-performance bio-based wood adhesives: A critical review. *J. Mater. Res. Technol.* **2022**, *21*, 3909−3946.
(21) Jiang, W.; Hosseinpourpia, R.; Biziks, V.; Ahmed, S. A.; Militz, H.; Adamopoulos, S. Preparation of Polyurethane Adhesives from Crude and Purified Liquefied Wood Sawdust. *Polymers* **2021**, *13*, 3267.
(22) Gosz, K.; Kowalkowska-Zedler, D.; Haponiuk, J.; Piszczyk, Ł. Liquefaction of alder wood as the source of renewable and sustainable polyols for preparation of polyurethane resins. *Wood Sci. Technol.* **2020**, *54*, 103−121.
(23) Lee, W.-J.; Lin, M.-S. Preparation and application of polyurethane adhesives made from polyhydric alcohol liquefied Taiwan acacia and China fir. *J. Appl. Polym. Sci.* **2008**, *109*, 23−31.
(24) Jiang, W.; Kumar, A.; Adamopoulos, S. Liquefaction of lignocellulosic materials and its applications in wood adhesives—A review. *Ind. Crops Prod.* **2018**, *124*, 325−342.
(25) Hernandez, C.; Maranon, A.; Ashcroft, I. A.; Casas-Rodriguez, J. P. A computational determination of the Cowper−Symonds parameters from a single Taylor test. *Appl. Math. Model.* **2013**, *37*, 4698−4708.
(26) Karpiesiuk, J. Young's Modulus and Poisson's Ratio of Polyurethane Adhesive in Lightweight Floor System. *Mod. App. Mater. Sci.* **2020**, *2*, 251.
(27) Chen, W. F.; Saleeb, A. F. *Constitutive Equations for Engineering Materials: Elasticity and Modeling*; Elsevier Science, 2013.
(28) Korobeynikov, S. N. Analysis of Hooke-like isotropic hypoelasticity models in view of applications in FE formulations. *Arch. Appl. Mech.* **2020**, *90*, 313−338.
(29) Acuña, L.; Martínez, R.; Spavento, E.; Casado, M.; Álvarez-Martínez, J.; O'Ceallaigh, C.; Harte, A. M.; Balmori, J.-A. Modulus of elasticity prediction through transversal vibration in cantilever beams and ultrasound technique of different wood species. *Constr. Build. Mater.* **2023**, *371*, 130750.
(30) Wang, Y.; Han, Y.; Hu, W.; Fu, D.; Wang, G. Analytical strategies for chemical characterization of bio-oil. *J. Sep. Sci.* **2020**, *43*, 360−371.
(31) Lee, P. S.; Kim, S.-C.; Tikue, E. T.; Jung, S. M. One-Pot Reaction of Waste PET to Flame Retardant Polyurethane Foam, via Deep Eutectic Solvents-Based Conversion Technology. *J. Polym. Environ.* **2022**, *30*, 333−343.
(32) Cinelli, P.; Anguillesi, I.; Lazzeri, A. Green synthesis of flexible polyurethane foams from liquefied lignin. *Eur. Polym. J.* **2013**, *49*, 1174−1184.
(33) Roldán-San Antonio, J. E.; Martín-Hernández, E.; Briones, R.; Martín, M. Process design and scale-up study for the production of polyol-based biopolymers from sawdust. *Sustain. Prod. Consum.* **2021**, *27*, 462−470.
(34) Cevher, D.; Sürdem, S. Polyurethane adhesive based on polyol monomers BHET and BHETA depolymerised from PET waste. *Int. J. Adhes. Adhes.* **2021**, *105*, 102799.
(35) Sheinbaum, M.; Sheinbaum, L.; Weizman, O.; Dodiuk, H.; Kenig, S. Toughening and enhancing mechanical and thermal properties of adhesives and glass-fiber reinforced epoxy composites by brominated epoxy. *Composites, Part B* **2019**, *165*, 604−612.
(36) McDevitt, N. T.; Baun, W. L. The Three-Point Bend Test for Adhesive Joints. In *Adhesive Joints: Formation, Characteristics, and Testing*; Mittal, K. L., Ed.; Springer US: Boston, MA, 1984; pp 381−394.
(37) Holmberg, S.; Persson, K.; Petersson, H. Nonlinear mechanical behaviour and analysis of wood and fibre materials. *Comput. Struct.* **1999**, *72*, 459−480.
(38) Rana, D.; Lee, C. H.; Cho, K.; Lee, B. H.; Choe, S. Thermal and mechanical properties for binary blends of metallocene polyethylene with conventional polyolefins. *J. Appl. Polym. Sci.* **1998**, *69*, 2441−2450.
(39) Rana, D.; Cho, K.; Woo, T.; Lee, B. H.; Choe, S. Blends of ethylene 1-octene copolymer synthesized by Ziegler−Natta and metallocene catalysts. I. Thermal and mechanical properties. *J. Appl. Polym. Sci.* **1999**, *74*, 1169−1177.
(40) Rana, D.; Kim, H. L.; Kwag, H.; Choe, S. Hybrid blends of similar ethylene 1-octene copolymers. *Polymer* **2000**, *41*, 7067−7082.
(41) Rana, D.; Kim, H. L.; Kwag, H.; Rhee, J.; Cho, K.; Woo, T.; Lee, B. H.; Choe, S. Blends of ethylene 1-octene copolymer synthesized by Ziegler−Natta and metallocene catalysts. II. Rheology and morphological behaviors. *J. Appl. Polym. Sci.* **2000**, *76*, 1950−1964.
(42) Malik, M.; Kaur, R. Influence of aliphatic and aromatic isocyanates on the properties of poly(ether ester) polyol based PU adhesive system. *Polym. Eng. Sci.* **2018**, *58*, 112−117.
(43) de Souza, F. M.; Kahol, P. K.; Gupta, R. K. Introduction to Polyurethane Chemistry. In *Polyurethane Chemistry: Renewable Polyols and Isocyanates*; American Chemical Society, 2021; Vol. *1380*, pp 1−24.
(44) Borrero-López, A. M.; Valencia, C.; Domínguez, G.; Eugenio, M. E.; Franco, J. M. Rheology and adhesion performance of adhesives formulated with lignins from agricultural waste straws subjected to solid-state fermentation. *Ind. Crops Prod.* **2021**, *171*, 113876.
(45) Todorovic, T.; Norström, E.; Khabbaz, F.; Brücher, J.; Malmström, E.; Fogelström, L. A fully bio-based wood adhesive valorising hemicellulose-rich sidestreams from the pulp industry. *Green Chem.* **2021**, *23*, 3322−3333.
(46) Bockel, S.; Harling, S.; Grönquist, P.; Niemz, P.; Pichelin, F.; Weiland, G.; Konnerth, J. Characterization of wood-adhesive bonds in wet conditions by meansof nanoindentation and tensile shear strength. *Eur. J. Wood Wood Prod.* **2020**, *78*, 449−459.
(47) Ramesh, M.; Rajeshkumar, L.; Sasikala, G.; Balaji, D.; Saravanakumar, A.; Bhuvaneswari, V.; Bhoopathi, R. A Critical Review on Wood-Based Polymer Composites: Processing, Properties, and Prospects. *Polymers* **2022**, *14*, 589.
(48) Maulana, M. I.; Lubis, M. A. R.; Febrianto, F.; Hua, L. S.; Iswanto, A. H.; Antov, P.; Kristak, L.; Mardawati, E.; Sari, R. K.; Zaini, L. H.; Hidayat, W.; Giudice, V. L.; Todaro, L. Environmentally

https://doi.org/10.1021/acsomega.3c04393
ACS Omega 2023, 8, 38178−38190

Friendly Starch-Based Adhesives for Bonding High-Performance Wood Composites: A Review. *Forests* **2022**, *13*, 1614.
(49) Hellmayr, R.; Bischof, S.; Wühl, J.; Guebitz, G. M.; Nyanhongo, G. S.; Schwaiger, N.; Liebner, F.; Wimmer, R. Enzymatic Conversion of Lignosulfonate into Wood Adhesives: A Next Step towards Fully Biobased Composite Materials. *Polymers* **2022**, *14*, 259.
(50) Ebnesajjad, S. Chapter 5 - Theories of Adhesion. In *Surface Treatment of Materials for Adhesive Bonding*; Ebnesajjad, S., Ed., 2nd ed.; William Andrew Publishing: Oxford, 2014; pp 77−91.
(51) Ebnesajjad, S.; Landrock, A. H. Chapter 1 - Introduction and Adhesion Theories. In *Adhesives Technology Handbook*; Ebnesajjad, S., Landrock, A. H., Eds., 3rd ed.; William Andrew Publishing: Boston, 2015; pp 1−18.
(52) Omairey, S.; Jayasree, N.; Kazilas, M. Defects and uncertainties of adhesively bonded composite joints. *SN Appl. Sci.* **2021**, *3*, 769.
(53) Atakok, G.; Kam, M.; Koc, H. B. Tensile, three-point bending and impact strength of 3D printed parts using PLA and recycled PLA filaments: A statistical investigation. *J. Mater. Res. Technol.* **2022**, *18*, 1542−1554.
(54) Boutar, Y.; Naïmi, S.; Mezlini, S.; Carbas, R. J. C.; da Silva, L. F. M.; Ben Sik Ali, M. Cyclic fatigue testing: Assessment of polyurethane adhesive joints' durability for bus structures' aluminium assembly. *J. Adv. Join. Process.* **2021**, *3*, 100053.

https://doi.org/10.1021/acsomega.3c04393
ACS Omega 2023, 8, 38178−38190